This article has not been copyedited and formatted. The final version may differ from this version.
DMD Fast Forward. Published on May 24, 2012 as doi:10.1124/dmd.112.044792

Development of a Carbon-14 Labeling Approach to Support Disposition Studies with a Pegylated Biologic

Haiqing Wang, Lifei Wang, Kai Cao, Stuart L. Emanuel, Paul Morin, Zheng Lin, Guoxiang Shen, Jennifer Hosbach, Donglu Zhang, Samuel Bonacorsi, A. David Rodrigues, Zheng Yang

Pharmaceutical Candidate Optimization (*H.W., L.W., G.S., D.Z., A.D.R., Z.Y.*), Chemistry (*K.C., S.B.*), Biology (*S.L.E., J.H.*), Protein Science and Structure (*P.M., Z.L.*), Bristol-Myers Squibb Research & Development, Princeton, New Jersey

DMD Fast Forward. Published on May 24, 2012 as DOI: 10.1124/dmd.112.044792
This article has not been copyedited and formatted. The final version may differ from this version.

Running Title: Tissue Distribution of a [^{14}C]-labeled PEGylated Adnectin

Corresponding author:

Haiqing Wang, Ph.D.

Metabolism and Pharmacokinetics

Pharmaceutical Candidate Optimization

Bristol-Myers Squibb Research & Development

Route 206 & Province Line Rd,

Princeton, NJ 08543

Telephone: 609-252-4532

Fax: 609-252-6802

Email: haiqing.wang@bms.com

Document Summary:

Number of text pages: 35

Number of tables: 2

Number of figures: 4

Number of references: 27

Number of words in the Abstract: 218

Number of words in the Introduction: 749

Number of words in the Discussion: 1393

ABBREVIATIONS: BMPS, N-(ß-maleimidopropyloxy)succinimide; DIC, N,N'-diisopropylcarbodiimide; ECL, electrochemiluminescence; EGFR, epidermal growth factor receptor; EI-tandem, Anti-EGFR and IGF-1R tandem Adenctin; ELISA, Enzyme-linked immunosorbent assay; IGF-1R, anti-insulin-like growth factor 1 receptor; IV, intravenous; IP, intraperitoneal; Ni-NTA, Nickel-nitrilotriacetic acid; PEG, polyethyleneglycol; P40B, 2-branch 40kDa PEG; P40B-NH2, 2-branch 40kDa PEG-propylamine; QWBA, quantitative whole-body autoradiography; SDS-PAGE, sodium dodecyl sulfate polyacrylamide gel electrophoresis; SPR, surface plasmon resonance; TEA, triethylamine; TGI, tumor growth inhibition; %ID/g, Percentage injected dose per gram of tissue.

ABSTRACT

Although it is widely accepted that one can extend the pharmacokinetic half-life of a therapeutic protein by covalent conjugation with polyethylene glycol (PEG), the disposition properties of such biologics have not yet been fully evaluated. Therefore, a novel [^{14}C]-labeling method was developed that can be applied to a biologic conjugated with PEG through a maleimide-cysteine reaction. The method was used to study the tissue and tumor distribution of a PEGylated Adnectin™, a recombinant protein derived from the tenth type III domain of fibronectin, in nude mice bearing human xenograft tumors. The PEGylated Adnectin contained a 40-kDa branched PEG (P40B) that was labeled with [^{14}C] at the linker region between the PEG and Adnectin, without compromising cellular activity and plasma half-life in mice. Following a single intravenous or intraperitoneal dose (33 mg/kg, 1.7 μCi/mouse) of [^{14}C]-P40B-Adnectin, quantitative whole-body autoradiography analysis revealed that the liver had the highest uptake of the radioactivity among non-tumor tissues, followed by the kidneys and lung. The muscle and brain showed the least penetration of the radioactivity among all tissues examined. In addition, the [^{14}C]-P40B-EI-tandem penetrated into the tumor tissue, although the extent of accumulation was largely dependent on tumor type. Therefore, it was possible to assess the tissue distribution of a PEGylated biologic after it had been [^{14}C]-labeled using the novel method described herein.

INTRODUCTION

For most therapeutic proteins, it is known that one can extend the pharmacokinetic half-life, and hence reduce the dosing frequency, by covalent conjugation with polyethylene glycol (PEG). The PEG moiety increases the hydrodynamic radius of the protein and shields it from the immune system, thus reducing the potential for immunogenicity. A larger hydrodynamic radius also may slow renal excretion, prolong half-life, and shield the protein from various proteolytic enzymes (Jevsevar et al., 2010; Bailon et al., 2009; Gaberc-Porekar et al., 2008). To date, nine "PEGylated" biologics have been approved for clinic use, with many others currently under development. The majority of commercial PEGylated biologics are recombinant human proteins, such as PEG-interferons for the treatment of hepataitis C. Recently, certolizumab pegol (Cimzia®), a PEGylated anti-TNFα antibody fragment (Fab), was approved for the treatment of rheumatoid arthritis and Crohn's disease (Veronese et al., 2008). The approval of Cimzia demonstrated the potential of PEGylated biologics as an alternative to conventional therapeutic monoclonal antibodies.

Various protein scaffolds have emerged as a new generation of biologics complementing the existing therapeutic antibodies for the treatment of cancer and other chronic disorders. The protein scaffolds are small proteins consisting of a natural backbone derived from human proteins and a flexible targeting domain that is engineered to specifically recognize a therapeutic target of interest (Gebauer et al., 2009; Skerra, 2007). For example, Adnectins are a class of protein scaffolds derived from the tenth type III domain of human fibronectin, an extracellular protein abundant in human serum and the extracellular space. By changing the amino acid sequence of three targeting

DMD Fast Forward. Published on May 24, 2012 as DOI: 10.1124/dmd.112.044792
This article has not been copyedited and formatted. The final version may differ from this version.

loops but keeping the scaffold intact, these small proteins (~10 kDa) can bind to specific disease targets with an affinity and specificity comparable to or better than those of antibodies (Lipovsek, 2011; Emanuel et al., 2011). To prolong the residence time of these small-size protein scaffolds in the body, a variety of novel approaches, such as Fc fusions and albumin binding, are being tested (Gay et al., 2010; Hopp et al., 2010). Nevertheless, PEGylation is still the most reliable and established technology for the extension of pharmacokinetic half-life. For example, the plasma half-life of CT-322, an Adnectin conjugated with a 40-kDa branched PEG, is ~64 h in cancer patients (Tolcher et al., 2011). The half-life is longer (~64 vs 1-5 h) than that of non-PEGylated proteins, such as rhGM-CSF (18 kDa), rhIL-3 (15 kDa), and rhIFN-α2a (19kDa) (Hovgaard et al., 1992 and 1994; Taguchi et al., 1986).

Although it has been widely accepted that the pharmacokinetics of PEGylated biologics is mostly driven by the size of PEG, the disposition properties of such biologics have not yet been fully evaluated. This is possibly due to the difficulties of quantifying PEGylated biologics in different tissues. For example, several labeling methods are available for protein therapeutics, including iodine-125 (^{125}I) and fluorescent labeling, as well as positron emission tomography (PET) tracers (Niu et al., 2009; Hoeben et al., 2011). However, these methods inevitably change the overall structure of the biologic in question. In most cases where the random conjugation is used as the cross-linking chemistry, the resulting product contains heterogenous species and there is an increased risk that biological and pharmacokinetic properties are altered. In addition, the radionuclide-conjugated biologics require immediate *in vivo* assessment due to possible radiolysis during storage and the short half-life of the PET tracers. The need for special

laboratory protection and instrumentation further complicates disposition studies employing the aforementioned labeling approaches. Therefore, a sensitive but convenient labeling method has been sought to support distribution studies with PEGylated biologics. Such distribution data would be useful and enable one to assess differential uptake into target and non-target (e.g., clearance) tissues and further support efficacy and toxicity assessment.

Towards this end, a novel [^{14}C]-labeling method was developed that can be applied to any protein scaffold conjugated with a PEG via a cysteine residue. Compared to the existing labeling methods, this approach is easy to use. In addition, the labeled molecule shares the same structure as the non-labeled version, and is generally stable due to the [^{14}C]-label as a low energy β-emitter with a long half-life. It was possible to subsequently apply the approach to a 40-kDa branched PEGylated Adnectin (P40B-EI-tandem) that targets both EGFR and IGF-1R (Fig. 1). The anti-tumor efficacy of P40B-EI-tandem was demonstrated in various human xenograft tumor models that express EGFR and/or IGF-1R. In the present study, the tissue distribution and tumor uptake of P40B-EI-tandem was investigated using QWBA following a single IV and IP dose of [^{14}C]-P40B-EI-tandem.

MATERIALS AND METHODS

Reagents. All commercial reagents used for synthesis were purchased from Sigma-Aldrich (St. Louis, MO). 1, 4-[^{14}C]-labeled maleic acid (55 mCi/mmol) was obtained from PerkinElmer Life Sciences Inc. (Boston, MA). Ecolite scintillation mixture was obtained from MP Biomedicals (Irvine, CA). 40-kDa branched PEG-propylamine (P40B-NH2) and maleimide-activated 40-kDa branched PEG (for synthesis of the non-labeled agent) were purchased from NOF America Corporation (White Plains, NY). Disposable G-25 PD-10 columns and Hi-Trap SP columns were obtained from GE Healthcare Bio-Sciences (Piscataway, NJ). Ni-NTA agarose resin was purchased from Qiagen (Valencia, CA), and Sartobind Q 75 filters were acquired from Sartorius Stedim Biotech (Aubagne, France).

Synthesis of [^{14}C]-Labeled Cross-Linker ([^{14}C]-BMPS). Preparation of [^{14}C]-BMPS was accomplished in two steps as shown in Fig. 2A. The starting materials 3-aminopropanoic acid (98 mg, 1.1 mmol) and [1,4-^{14}C]-maleic acid (118 mg, 1.0 mmol, specific activity 55 mCi/mmol) were dissolved in 3.5 mL of dioxane and heated to 110°C for 18 h in the presence of phosphorouspentoxide (P_2O_5, 156 mg, 1.1 mmol). The reaction mixture was then filtered while it was hot. The crude product mixture was purified on a 21.2 x 250 mm Synergy Hydro-RP column Phenomenex (Torrance, CA), using the following separation condition: flow rate = 16 mL/min; UV wavelength = 220 nm; mobile phase solvent A = water (0.1% TFA); mobile phase solvent B = acetonitrile (0.1% TFA); flow gradient = 10% B in A @ 0 min, 40% B in A @ 10 min:, 95% B in A @ 15 min, 10% B @ 20 min; retention time = 8.4 min. 4-([1,4-^{14}C]-maleimido)propanoic acid (34 mg) was obtained after evaporation (Alagic A., et. al.,

2005). The dried product (34 mg, 0.20 mmol) and N-hydroxysuccinimide (29 mg, 0.25 mmol) were dissolved in cooled DMF (1 mL) submerged in an ice-bath. N,N'-diisopropylcarbodiimide (DIC) (0.062 ml, 0.40 mmol) was added to the solution and the mixture was stirred for 3 h. Dichloromethane (20 mL) was then added to the reaction mixture followed by filtration to remove urea. The organic layer was then washed with water (5 mL x 2), dried over Na_2SO_4 and filtered. The product ([^{14}C]-BMPS; 56 mg, 12 mCi) was obtained after evaporation and its specific activity was determined by gravimetric analysis (56 mCi/mmol).

Purification of EI-Tandem. The construction and characterization of the EI-tandem was reported previously (Emanuel et al., 2011). The 23-kDa recombinant protein was produced by covalently linking an EGFR-binding Adnectin to the C-terminus of an IGF-IR-binding Adnectin using a glycine-serine linker (Fig. 1). The protein was expressed as a C-terminus His_6-tag fusion for affinity purification. To conjugate with PEG, a serine to cysteine mutation was introduced into the protein near the C-terminus. The protein was over-expressed in *E. Coli,* and purified using Ni-NTA agarose resin following the manufacture's instructions. The purified EI-tandem was eluted from the Ni-NTA resin using Na_2HPO_4 (20 mM, pH 8.0) buffer containing 400 mM NaCl and 400 mM imidazole and immediately coupled with [^{14}C]-labeled maleimide-activated 40-kDa branched PEG ([^{14}C]-maleimide-PEG) as described below.

Synthesis of [^{14}C]-Maleimide-PEG and Subsequent PEGylation. The reaction procedure of [^{14}C]-maleimide-PEG synthesis and the subsequent PEGylation with purified EI-tandem were outlined in Fig. 2B. [^{14}C]-BMPS (5 mg, 20 μmol, 1 mCi) was dissolved in 4 mL of CH_2Cl_2 and transferred to a glass vial containing 40-kDa branched

DMD Fast Forward. Published on May 24, 2012 as DOI: 10.1124/dmd.112.044792
This article has not been copyedited and formatted. The final version may differ from this version.

PEG-propylamine (P40B-NH2, 160 mg, 4 μmol) powder. After the addition of triethylamine (TEA, 14 μL, 100 μmol), the reaction mixture was stirred at room temperature for 4 h. The solvent was then evaporated to dryness under a stream of nitrogen. The residue was re-suspended in a 2 mL Tris buffer (10 mM, pH 7.0) to quench the amine-coupling reaction. The un-reacted [^{14}C]-BMPS and other small molecule byproducts were removed by applying the mixture onto a G-25 PD-10 column pre-equilibrated with the Tris buffer (10 mM, pH 7.0). The eluate containing [^{14}C]-maleimide-PEG was conjugated with the freshly purified EI-tandem, through a maleimide and cysteine reaction to yield [^{14}C]-P40B-EI-tandem. The reaction mixture was incubated at room temperature for 2 h. Progress of the PEGylation was confirmed by SDS-PAGE (Fig. 2C). The reaction mixture was dialyzed into a 50 mM NaAc buffer (pH 4.5) for purification using cation exchange chromatography (see below).

SDS-PAGE. The PEGylated and non-PEGylated EI-tandem were separated using a Novex mini-gel electrophoresis system (Invitrogen, Carlsbad CA). The protein samples were denatured after adding lithium dodecyl sulfate (LDS) sample buffer and heating at 70 ºC for 5 min. Samples (15-20 uL) were subsequently loaded onto a pre-cast 10% NuPAGE® Bis-Tris Gel and subjected to electrophoresis in SDS-MES (2-[N-morpholino] ethane sulfonic acid) running buffer at 200V for 45 min. Gels were stained using Simply Blue Safestain (Invitrogen, Carlsbad CA). The moleculear weight of the protein bands was estimated by comparing with the Novex® Sharp Protein Standards. All reagents for the SDS-PAGE were obtained from Invitrogen (Carlsbad CA).

Purification of [^{14}C]-P40B-EI-tandem. [^{14}C]-P40B-EI-tandem was purified by cation exchange chromatography. Briefly, the dialyzed mixture was clarified by centrifugation

and loaded on to a HiTrap Sulfopropyl (SP) sepharose column pre-equilibrated with the 50 mM NaAc buffer at pH 4.5 (buffer A). The column was washed with buffer A to remove the un-conjugated PEG. The PEGylated vs. non-PEGylated proteins were separated and eluted with a linear gradient of 0-0.5 M NaCl in buffer A. The fractions containing [^{14}C]-P40B-EI-tandem were pooled, concentrated and buffer-exchanged to Dulbecco's PBS buffer (pH 7.2). Lipo-polysaccharides were removed with Sartobind Q charged membranes following manufacture's protocol. The purity of [^{14}C]-P40B-EI-tandem was checked by SDS-PAGE (Fig. 2C) and gel filtration analysis using a Shodex KW-803 size exclusion column (Showa Denko America, Inc, New York, NY) connected to a HPLC system with a radio-HPLC detector (Fig. 2D).

Concentration and Radioactivity Determination. The concentration of PEGylated and non-PEGylated proteins was determined by A280/A260 measurement using Nanodrop 1000 (Thermo Scientific, Wilmington, DE). Because PEG does not have a UV absorbance, the mass of the PEG portion in the PEGylated protein was not considerred. Consequently, a MW of 23 kDa (protein only) rather than that of 63 kDa (PEG+protein) was used to covert mass unit (mg/mL) to molar unit (nM or μM). To determine the total radioactivity of [^{14}C]-P40B-EI-tandem, the PEGylated protein (1-10 μL) was diluted to Ecolite scintillation mixture followed by radioactivity counting on a Beckman LS6000 liquid scintillation counter (Beckman Coulter Inc, Brea, CA). The specific activity was calculated to be 2.5 μCi/mg of protein (55 mCi/mmol).

Inhibition of IGF-IR/EGFR Phosphorylation in H292 cells. H292 cells (65,000 cells/well) were plated in 96-well plates and incubated overnight. After 24 h, cells were washed once and then incubated for 24 h in serum-free media. Serial dilutions of either

DMD Fast Forward. Published on May 24, 2012 as DOI: 10.1124/dmd.112.044792
This article has not been copyedited and formatted. The final version may differ from this version.

[^{14}C]-labeled or non-labeled P40B-EI-tandem were added, and cells were incubated for 3 h. Cells were stimulated with 100 ng/mL of IGF-I or EGF for 10 min at 37°C. Media was removed and cells were lysed in a 100-μL cell lysis buffer as described for immunoblotting (Emanuel et al., 2008; 2011). After 15 min incubation at room temperature, the lysate was subjected to an ELISA measuring phospho-IGF-IR (tyrosine 1131), or phospho-EGFR (tyrosine 1068), according to the manufacturer's procedure (Cell Signaling Technology Inc., Danvers, MA).

Animal Preparation and Dosing. Female athymic nude mice 5 to 6 weeks of age were obtained from Harlan Sprague Dawley, Inc. (Indianapolis, IN) and quarantined for 3 weeks prior to their use in experiments. Animals were provided food and water *ad libitum* and cared for according to the Association for Assessment and Accreditation of Laboratory Animal Care International and Bristol-Myers Squibb guidelines. Tumors were propagated by subcutaneous implantation of 1 mm^3 fragments in nude mice. The RH41 tumor was implanted in the right hind flank two weeks prior to the implantation of the H292 tumor in the left hind flank. When the tumor sizes reached 300 mm^3, the mice were dosed IV or IP with 33 mg/kg of [^{14}C]-P40B-EI-tandem (total radioactivity 1.7 μCi/mouse). Two mice from each group were sacrificed at 2, 24, 48, and 53 h after IV dosing or 8, 48 and 53 h after IP dosing. The serum samples were collected for exposure analysis. One mouse each after IV (2, 24, and 53 h) and IP (8 and 53 h) dosing was used for QWBA analysis.

Analysis of [^{14}C]-P40B-EI-Tandem in Serum. The serum concentration of [^{14}C]-P40B-EI-tandem was determined by ELISA. The recombinant biotinylated IGF-1R (Bristol-Myers Squibb, Lawrenceville NJ) was coated on a 96-well streptavidin plate at a

DMD Fast Forward. Published on May 24, 2012 as DOI: 10.1124/dmd.112.044792
This article has not been copyedited and formatted. The final version may differ from this version.

final concentration of 0.5 µg/mL. [^{14}C]-P40B-EI-tandem from mouse serum was captured onto the plate. After a washing step, the captured [^{14}C]- P40B-EI-tandem was detected by an anti-PEG monoclonal rabbit antibody (Epitomics, Burlingame, CA) that was subsequently detected by a sulfo tag-conjugated anti-rabbit polyclonal antibody. The concentrations were calculated based on the electrochemiluminescence of the sample compared to a 4-parameter fit of a standard curve. The dynamic range of the assay is 0.8-200 nM, with a lower limit of quantification (LLQ) of 1 nM.

Analysis of serum concentration of radioactivity. An aliquot of 10 µL serum sample was diluted 10-fold to 100 µL. The diluted serum (20 µL) was added to a scintillation vial containing 5 mL of Ecolite scintillation mixture followed by radioactivity counting on a Beckman LS6000 liquid scintillation counter (Beckman Coulter Inc, Brea CA). The resulting dpm values were converted to the radioactivity concentration using the equation below:

$$[Radioactivity](\mu M) = \frac{dpm \times 10^6}{2\ \mu L \times 2.22 \times 10^6 \left(\frac{dpm}{\mu Ci}\right) \times 2.5\ \left(\frac{\mu Ci}{mg}\right) \times 23000\,(Da)}$$

where the 2 µL is the serum volume, 2.22 x10^6 dpm/µCi is the conversion factor, 2.5 µCi/mg is the specific activity, and the 23000 Da is the molecular weight.

QWBA. The whole-body sections of the frozen mouse carcasses were taken at 40 µm thick in the sagittal plane and were captured on an adhesive tape (Scotch Tape No. 8210, 3M Ltd., St. Paul, MN, USA) at -20°C. Sections at various levels were collected to include the major tissues and tumors, and then were dried in the cryomicrotome at -20°C for 48 h. The sections of each mice were mounted on a cardboard, covered with a thin plastic wrap, and exposed along with a calibration standard of [^{14}C]-glucose at 14

different concentrations (range from ~0 to 0.8 μCi/g) to a [^{14}C]-sensitive phosphor imaging plate (Fuji Biomedical, Stamford, CT). The exposure experiment was conducted in light-tight exposure cassettes for 5 days at room temperature in a lead shielding box. After exposure, the imaging plates were scanned using the Fuji FLA-3000 image acquisition system (Fuji Biomedical, Stamford, CT). The image files were processed using MCID image analysis software (v. 7.0, Imaging Research, Inc., St. Catherines, Ontario, Canada), and a standard curve was constructed from the integrated response and the radioactivity concentrations of the [^{14}C]-calibration standard. The LLQ was determined to be 0.5 nCi/g.

RESULTS

Design and Preparation of [^{14}C]-P40B-EI-Tandem. The cartoon structure of the P40B PEGylated EI-tandem was illustrated in Fig. 1. It was constructed as two tandemly-connected Adnectins with the N-terminus unit specifically bound to IGF-IR and the C-terminus unit bound to EGFR. A serine to cysteine mutation was introduced near the C-terminus to enable site-specific PEGylation. It was shown that the binding affinities of the EI-tandem to IGF-1R and EGFR were not compromised after the mutation (Emanuel et al., 2011). The EI-tandem Adnectin and PEG were covalently linked via a thioether and an amide bond. To form this linkage, a bi-functional cross linker (BMPS) was used (Fig. 1). The linker reacted with the 40-kDa branched PEG-propylamine (P40B-NH_2) via a succinimide-amine coupling reaction and with cysteine in the EI-tandem Adnectin via a maleimide-thiol reaction. The synthesis of the bi-functional cross linker is described under *Materials and Methods* using 1, 4-[^{14}C]-maleic acid as the starting material to introduce the [^{14}C]-label (Fig. 2A). The specific activity of the resulting [^{14}C]-BMPS was 55 mCi/mmol.

The [^{14}C]-P40B-EI-tandem was prepared via a two-step process (Fig. 2B). First, the P40B-NH_2 was conjugated with an excess amount of [^{14}C]-BMPS in CH_2Cl_2 under basic conditions by the addition of TEA. After completion of the reaction, the organic solvent was removed via evaporation, and the product was dissolved in a PBS buffer. The product, [^{14}C]-maleimide-PEG, shares the same structure as the non-radiolabeled version available from NOF America Corporation (White Plain, NY) for the routine site-specific PEGylation of proteins. The residual [^{14}C]-BMPS was removed by ultrafiltration prior to the subsequent conjugation with the EI-tandem Adnectin. In parallel with the

DMD Fast Forward. Published on May 24, 2012 as DOI: 10.1124/dmd.112.044792
This article has not been copyedited and formatted. The final version may differ from this version.

[^{14}C]-maleimide-PEG synthesis, the EI-tandem Adnectin was purified by subjecting *E. Coli* lysate to Ni-NTA affinity chromatography. To avoid inter-molecule disulfide formation, the purified protein was immediately conjugated with the [^{14}C]-maleimide-PEG through the maleimide-thiol reaction to yield [^{14}C]-P40B-EI-tandem. The PEGylation reaction was monitored by SDS-PAGE (Fig. 2C), where the coomassie blue-stained protein band was shifted from below 30 kDa for the EI-tandem Adnectin to above 100 kDa after PEGylation. The apparent higher mass is typical of a PEGylated protein on a SDS-PAGE gel (Sato, 2002). The PEGylated product, [^{14}C]-P40B-EI-tandem, was further purified on a HiTrap cation exchange column to ensure electrophoretic homogeneity (Fig. 2C). The purity and specific radioactivity were verified by size-exclusion chromatography (Fig. 2D). Both UV (A280 nm) and radioactivity traces showed a single peak eluted at 15 min, suggesting the radioactivity was nearly 100% in the final purified product. Lipo-polysaccharides were subsequently removed from the final purified PEGylated protein by Sartobind Q 75-filter. The specific activity was determined to be 2.5 μCi/mg of protein (55 mCi/mmol).

The non-radiolabled P40B-EI-tandem was prepared following the same procedure as the [^{14}C]-radiolabeled version, except that the purified EI-tandem was directly conjugated with the maleimide-activated PEG purchased from NOF.

Inhibition of Receptor Phosphorylation by the [^{14}C]-P40B-EI-Tandem. The inhibitory potency of [^{14}C]-P40B-EI-tandem was evaluated in the H292 lung cancer cell line. The H292 cell line was selected due to its high level expression of both EGFR and IGF-1R and sensitivity to growth inhibition by anti-EGFR agents. As shown in Fig. 3A and B, [^{14}C]-P40B-EI-tandem inhibited EGF-stimulated EGFR phosphorylation with an

DMD Fast Forward. Published on May 24, 2012 as DOI: 10.1124/dmd.112.044792
This article has not been copyedited and formatted. The final version may differ from this version.

IC_{50} of 23 nM, and blocked IGF-stimulated IGF-1R phosphorylation with an IC_{50} of 0.3 nM. The inhibitory potency was equivalent to the non-radiolabeled P40B-EI-tandem tested in the same experiment (Figs. 3A and B) and nearly identical to the previously reported IC_{50} values of 31 (blocking EGFR) and 0.2 nM (blocking IGF-1R) (Emanuel et al., 2011). The results clearly demonstrated that the [^{14}C]-label introduced in the linker region did not affect the cellular potency of the PEGylated EI-Adnectin.

Pharmacokinetics and Tissue Distribution of [^{14}C]-P40B-EI-Tandem in H292 and RH41 Tumor-Bearing Mice. The H292 and RH41 cell-derived tumor fragments were implanted in athymic mice on either side of the hind flank. In contrast to H292 cells that are sensitive to both EGFR and IGF-1R signaling, the proliferation of RH41 Ewing sarcoma cells are driven predominantly by IGF-1R signaling and not sensitive to EGFR blockade. When both tumors had grown to ~ 300 mm^3, [^{14}C]-P40B-EI-tandem was administered IV or IP (33 mg/kg, 1.7 µCi/mouse).

The serum concentration of [^{14}C]-P40B-EI-tandem after IV and IP administration was determined by ELISA. Following the IP administration, the average concentrations after dose adjustment were 0.27 and 0.066 µM/mg/kg at 8 and 48 h, respectively (Table 1). The dose normalized exposures were in-line with those of the non-labeled P40B-EI-Adnectin after 10 and 100 mg/kg IP administration, which were 0.27-0.33 and 0.044-0.077 µM/mg/kg at 8 and 48 h, respectively (Emanuel et al., 2011). The comparable exposures suggest similar in vivo stability of the [^{14}C]-labeled and the non-labeled P40B-EI-Adnectin, consistent with the in vitro findings.

The serum concentrations of radioactivity were also measured (Table 1). The radioactivity concentrations were systematically ~ 2-fold (1.7-2.4 fold) higher than the

concentrations determined by the ELISA method, which, we believe, is largely due to the systemic error between the two analytical methods. Nevertheless, there appeared to be a trend of increase in the ratios from 1.7-fold at 2 and 24 h to 2.4-fold at 53 h, indicating the protein portion of the PEGylated tandem EI-Adnectin may be degraded and/or inactivated over the study duration. Assuming 100% of the radioactivty is from the intact P40B-EI-Adnectin at 2 h, approximately 30% [(2.4-1.7)/2.4*100% = 30%] of the radioactivity concentration may come from circulating PEGylated fragment at 53 h. Further profiling is required to characterize the radioactive species in the serum.

At 2, 24, and 53 h after IV dosing, the distribution of radioactivity in mouse tissues was determined by QWBA (Table 2) and the images of the radioactivity distribution are shown in Fig. 4 (A, B and C). At 2 and 24 h, the highest radioactivity appeared in blood, followed by the lung. Significant radioactivity was also observed in the heart, liver, and kidneys. At 53 h, the radioactivity in the liver and kidneys was higher than that in the blood and lung. High radioactivity was also observed in some part of the skin, which is likely due to the comparative binding affinity of the EI-tandem to both mouse and human EGFR (Emanuel et al., 2011). Fig. 4E shows the relative radioactivity levels of [^{14}C]-EI-tandem Adnectin in major tissues at 2, 24, and 53 h after IV administration into the mice bearing both RH41 and H292 tumors. At each time point, the level of radioactivity in each tissue was normalized by the level in the blood to yield tissue-to-blood ratios. The ratios increased over time in the liver, kidneys and bone marrow, indicating the slow uptake of [^{14}C]-P40B-EI-tandem into these tissues. In contrast, the tissue-to-blood ratios for the lung and heart remained the same from 2 to 53 h, indicating the distribution of [^{14}C]-P40B-EI-tandem into these tissues reached

DMD Fast Forward. Published on May 24, 2012 as DOI: 10.1124/dmd.112.044792
This article has not been copyedited and formatted. The final version may differ from this version.

equilibrium within 2 h after IV dosing. At 2 and 24 h, the highest levels of radioactivity were observed in blood. However, at 53 h, the levels in the liver and kidneys were 1.7 and 1.2-fold higher than that in blood, suggesting the accumulation of [^{14}C]-P40B-EI-tandem in both tissues. The muscle and brain had much lower levels of radioactivity compared to other tissues. The highest tissue-to-blood ratios for the muscle and brain during the study were observed at 53 h (ratios = 0.1 and 0.03, respectively).

Similar tissue distribution patterns were observed after IP administration to the mice bearing the same kind of tumors (supplement Table S1, and Fig. S1A). The tissue-to-blood ratios increased 5 and 7-fold in the liver and kidneys, respectively, suggesting the substantial uptake of [^{14}C]-P40B-EI-tandem into these tissues over the time interval studied. At 53 h, the levels of radioactivity in the liver and kidneys were 2.0 and 1.3-fold higher than in blood, comparable to the values obtained after IV administration. The levels of radioactivity in the lung, heart, and bone marrow were similar, and no accumulation in these tissues was observed. The muscle and brain had the lowest levels of radioactivity among all the tissues analyzed, consistent with the results obtained after IV administration.

Tumor Uptake of [^{14}C]-P40B-EI-Tandem. The extent of radioactivity distribution into the RH41 and H292 tumor tissues appeared to be both time- and tumor-dependent. As shown in Fig 4D, the radioactivity in both tumors planted in the same mouse increased over time. At 2 and 24 h, the radioactivity located at the rim of the RH41 tumor, but penetrated into the tumor 2 days later. In contrast, a significant amount of radioactivity was detected in the H292 tumor as early as 2 h after IV administration, and the radioactivity in H292 tumor was 3- to 5-fold greater than that in the RH41 tumor during

the duration of the study (Figs. 4D and E).

The radioactivity in the tumors was compared with that in blood (Fig. 4E). For the H292 tumor, the tumor-to-blood radioactivity ratios increased from 0.2 to 0.4 during (2 to 24 h post dose). At 53 h, the accumulation of radioactivity in the H292 tumor became evident (1.7-fold higher than that in blood). The tumor-to-blood radioactivity ratios in the RH41 tumor, however, were less than 1.0 across the study duration, suggesting no accumulation of radioactivity in the tumor.

Similar time- and tumor-dependent uptake of [^{14}C]-P40B-ATI-910 was observed after IP administration (supplement Table S1 and Fig. S1). At 8 h post dose, the radioactivity in the tumors was lower than that in blood, with H292 and RH41 tumor-to-blood ratios of 0.3 and 0.1, respectively, indicating a slow tumor penetration of [^{14}C]-P40B-ATI-910. At 53 h post-dose, the accumulation of radioactivity was evident in the H292 tumor, with the tumor radioactivity 2.4-fold higher than that in blood. In contrast, the tumor-to-blood ratios of RH41 were less than 1.0, suggesting no accumulation of radioactivity in the tumor.

DISCUSSION

Therapeutic biologicals have expanded beyond conventional monoclonal antibodies and recombinant human proteins to include multiple classes of macromolecules (Gebauer et al., 2009; Skerra, 2007). Given the increased variety of scaffolds, numerous strategies have been employed to prolong the pharmacokinetic half-life, enhance exposure and reduce dosing frequency. For example, some biologics are targeted to bind the FcRn receptor and avoid lysozomal digestion. Others are conjugated

DMD Fast Forward. Published on May 24, 2012 as DOI: 10.1124/dmd.112.044792
This article has not been copyedited and formatted. The final version may differ from this version.

with PEG or albumin, leading to an increased hydrodynamic radius and decreased renal filtration. Monoclonal antibodies and small protein scaffolds fused with the Fc fragment are examples of the first strategy, whereas the latter is best exemplified by PEGylated biologics or albumin binders (Gebauer et al., 2009; Skerra, 2007; Bailon et al., 2009; Veronese et al., 2008).

Ideally, a therapeutic protein exhibits superior potency and optimal pharmacokinetic properties. But in reality, however, the parts of the molecule that govern pharmacokinetics can alter or diminish pharmacologic activity by creating steric hindrance and also impact distribution into target tissues. Conversely, the pharmacologically active parts of the molecule may give rise to accelerated clearance via target-mediated elimination. Therefore, it is important to understand the overall properties of any therapeutic protein and use the information to drive the rational design of viable clinical candidates (Fishburn, 2008). Consequently, there is a need to develop new tools and methods that support the conduct of radiolabel disposition studies. This is especially important when having to assess the uptake of the protein into a target organ or group of cells, link pharmacokinetics to pharmacological activity, support efficacy studies in animal models and evaluate toxicity in specific organs.

As described herein, it was possible to develop a convenient [^{14}C]-labeling approach for a mono-PEGylated biologic and then assess its tissue distribution in mice. The [^{14}C]-label was introduced at the linker region of the PEGylated biologic based on several considerations. First, the synthesis of the [^{14}C]-labeled bi-functional cross linker, [^{14}C]-BMPS, was straightforward. The reagent is applicable to most site-specific mono-PEGylations through the maleimide-cysteine reaction. Thus, the specific activity will be

DMD Fast Forward. Published on May 24, 2012 as DOI: 10.1124/dmd.112.044792
This article has not been copyedited and formatted. The final version may differ from this version.

consistent from batch-to-batch and among various PEGylated proteins. Secondly, the [^{14}C] label has little impact on biological activity since the labeled biologic has the same structure as the non-labeled version. Moreover, [^{14}C] is a low energy beta-emitter which is expected to cause much less radiolysis of the labeled protein compared to [^{125}I] and other similar high energy radionuclides (Chakrabarti et al., 1996). Lastly, although it is feasible to incorporate [^{14}C]-labeled amino acids during protein expression, the resulting radioactive protein would complicate purification and characterization. In addition, [^{14}C]-amino acids can be recycled after proteolysis and incorporated into endogenous proteins in the body, which may potentially confound the data interpretation. Therefore, we believe that labeling the linker region is a reasonable approach.

The caveat of the current labeling method is that the radioactivity signal may represent a mixture of both the intact and the degraded PEGylated fragments, as expected from any study employing radio-label material. In this study, the ratios of the radioactivity over the active P40B-EI-Adnectin concentration appeared to increase ~30% over the time, suggesting the presence of the circulating PEGylated fragments. Because the stability of the [^{14}C]-P40B-EI-and the non-labeled version is similar, the [^{14}C]-label could be utilized as a tracer and enable the profiling of sera and tissues.

Although antibodies have been considered as a “silver bullet” for targeted cancer therapy, the delivery of macromolecules to target cells in solid tumors poses a significant challenge. Extensive studies have been conducted in mouse xenograft models to understand the delivery of anti-EGFR antibodies, such as panitumumab and cetuximab, to the solid tumors (Cai et al., 2007; Niu et al., 2009; Hoeben et al., 2011; Nayak et al., 2010). Therefore, it was of interest to characterize the target delivery and disposition of

DMD Fast Forward. Published on May 24, 2012 as DOI: 10.1124/dmd.112.044792
This article has not been copyedited and formatted. The final version may differ from this version.

P40B-EI-tandem in mouse xenografts using the [^{14}C]-labeling approach. The H292 and RH41 xenografts were selected for the study based upon the previous results, where the P40B-EI-tandem demonstrated nearly complete tumor growth inhibition (94% TGI) in the H292 xenograft model, but less than 60% TGI in the RH41 model at the same dose level (100 mg/kg, IP, three times a week) (Emanuel et al., 2011). To understand whether the difference in sensitivity was related to the exposure level of the drug in tumor tissues, the H292 and RH41 tumors were implanted in the same mice in order to compare the tumor exposure at the same systemic exposure levels.

Following a single IV or IP dose of [^{14}C]-P40B-EI-tandem, the highest uptake of radioactivity in the H292 and RH41 tumors was 11 and 3.6% of injected dose (ID)/g, respectively, at 53 h post dose. The level is within the range (2 to 35% ID/g) of the maximum concentrations observed for [^{64}Cu]-1,4,7,10-Tetraazacyclododecane-*N,N′,N′,N″*-tetraacetic acid (DOTA) labeled cetuximab and panitumumab in various EGFR-expressing tumor models (Cai et al., 2007; Niu et. al., 2009). This result indicates that the PEGylated EI-tandem may face the same obstacle as the antibodies in penetrating into the tumor due to the hydrodynamic radius of the PEG. Comparing the radioactivity in the two tumor types, at similar systemic exposures, the accumulation in the H292 tumor was higher (3- to 5-fold) versus the RH41 tumor over the entire study period. The results appeared to correlate well with the better efficacy observed in the H292 tumor-bearing mice. However, it is unknown whether the higher level of accumulation in the H292 tumor was due to the expression of EGFR and IGF-1R in the tumors. Previous positron emission tomography-imaging studies with ceutximab in xenografts showed that the levels of the antibody detected in the tumor tissues did not correlate with the receptor

DMD Fast Forward. Published on May 24, 2012 as DOI: 10.1124/dmd.112.044792
This article has not been copyedited and formatted. The final version may differ from this version.

expression levels, but may be related to the degree of vasculation of the tumor tissues. This suggests that vessel density and vascular permeability may play an important role in the tumor uptake of macromolecules (Niu et al., 2009). Therefore, immunohistochemical assessment of EGFR and IGF-1R expression levels, as well as analysis of microvascular density markers (e.g., CD31), in the H292 and RH41 tumor tissues is warranted. Such data could prove useful when trying to evaluate possible uptake mechanisms.

The P40B-EI-tandem exhibited comparable binding affinity to mouse and human EGFR in vitro (unpublished data). Therefore, the distribution of the [^{14}C]-P40B-EI-tandem in mouse tissues may provide insights into the distribution in humans. In mice, the distribution of [^{14}C]-P40B-EI-tandem to the heart and lung was completed within first 2 h after IV administration. However, the radioactivity was slowly absorbed into the liver, kidneys and tumor tissues. At 53 h, the radioactivity accumulated in the liver was 11% ID/g, 1.7-fold higher than that in blood and representing the highest level among non-tumor tissues. Initially, the accumulation of [^{14}C]-P40B-EI-tandem in the liver was thought to be target specific, since a high expression level of EGFR was reported in the mouse liver using anti-EGFR DOTA affibody (Tolmachev et al., 2010). Moreover, a previous tissue distribution study with [^{125}I]-labeled single chain bi-specific anti-CD19 and CD3 diabody, formatted with 40-kDa PEG, did not show accumulation in the liver (Stork et al., 2009). However, a recent in-house study with a similar P40B-PEGylated protein that neither binds to mouse EGFR nor targets liver abundant proteins showed similar accumulation in the liver as that of [^{14}C]-P40B-EI-tandem. These results have lead to the hypothesis that the radioactivity accumulation in the liver may not be due to

the binding to mouse EGFR, but may be related to phagocytosis by liver (Kupffer) cells, similar to PEGylated lipsomes (Ishida et al., 2008).

In conclusion, a novel method has been developed for the [^{14}C]-labeling of a PEGylated EI-tandem Adnectin. Once labeled, it was possible to assess its tissue distribution and tumor uptake in xenograft mice. The [^{14}C]-labeled P40B-EI-tandem showed equivalent cellular activity and serum half-life in mice as the non-labeled version, suggesting the [^{14}C]-label in the linker region does not interfere with the pharmacokinetic and pharmacological properties of the molecule. After dosing [^{14}C]-P40B-EI-tandem to the athymic mice bearing both H292 and RH41 tumors, QWBA showed that the highest uptake of the radioactivity among non-tumor tissues was in the liver, followed by the kidneys and lung. The muscle and brain showed the least penetration of the radioactivity among all tissues. In addition, [^{14}C]-P40B-EI-tandem penetrated into the H292 and RH41 tumors, but the extent of accumulation was largely tumor-dependent. Collectively, the present study demonstrates the feasibility of applying this new [^{14}C]-labeling method to study the target and tissue distribution of a PEGylated biologic.

ACKNOWLEDGEMENT

The authors gratefully acknowledge the helpful suggestions made by Huadong Sun, PhD, Brad Maxwell, PhD, Murli Krishna, PhD, and James Bryson, PhD (Bristol-Myers Squibb). The authors also thank Jochem Gokemeijer, PhD (Bristol-Myers Squibb) for providing the exposure data that were firstly reported by Emanuel et al. (Emanuel et al., 2011).

Authorship Contributions

Participated in research design: H. Wang, L. Wang, Emanuel, Morin, and Bonacorsi.

Conducted experiments: H. Wang. L. Wang, Cao, Hosbach, Lin, and Shen.

Contributed new reagents or analytic tools: Cao.

Performed data analysis: H. Wang, Yang, L. Wang, and Zhang.

Wrote or contributed to the writing of the manuscript: H. Wang, Rodrigues, Yang, L. Wang, and Emanuel.

REFERENCES

Alagic A, Koprianiuk A, and Kluger R (2005) Hemoglobin-superoxide dismutase-chemical linkages that create a dual function protein. *J Am Chem Soc* **127**: 8036-8043.

Bailon P and Won CY (2009) PEG-modified biopharmaceuticals. *Expert Opin Drug Deliv* **6**: 1-16.

Cai W, Chen K, He L, Cao Q, Koong A, and Chen X (2007) Quantitative PET of EGFR expression in xenograft-bearing mice using ^{64}Cu-labeled cetuximab, a chimeric anti-EGFR monoclonal antibody. *Eur J Nucl Med Mol Imaging* **34**: 850-858

Chakrabarti MC, Le N, Paik CH, De Graff WG, Carrasquillo JA (1996) Prevention of radiolysis of monoclonal antibody during labeling. *J Nucl Med.* 37:1384-8.

Emanuel SL, Engle LJ, Chao G, Zhu RR, Cao C, Lin Z, Yamniuk AP, Hosbach J, Brown J, Fitzpatrick E, Gokemeijer J, Morin P, Morse BA, Carvajal IM, Fabrizio D, Wright MC, Das Gupta R, Gosselin M, Cataldo D, Ryseck RP, Doyle ML, Wong TW, Camphausen RT, Cload ST, Marsh HN, Gottardis MM, and Furfine ES (2011) A fibronectin scaffold approach to bispecific inhibitors of epidermal growth factor receptor and insulin-like growth factor-I receptor. *MAbs* **3**: 38-48.

Emanuel SL, Hughes TV, Adams M, Rugg CA, Fuentes-Pesquera A, Connolly PJ, Pandey N, Moreno-Mazza S, Butler J, Borowski V, Middleton SA, Gruninger RH, Story JR, Napier C, Hollister B, and Greenberger LM (2008) Cellular and in vivo activity of JNJ-28871063, a nonquinazoline pan-ErbB kinase inhibitor that crosses the blood-brain barrier and displays efficacy against intracranial tumors. *Mol Pharmacol* **73**:338-348.

Fishburn CS (2008) The pharmacology of PEGylation: balancing PD with PK to generate novel therapeutics. *J Pharm Sci* **97**: 4167-4183.

Gaberc-Porekar V, Zore I, Podobnik B, and Menart V (2008) Obstacles and pitfalls in the PEGylation of therapeutic proteins. *Curr Opin Drug Discov Devel* **11**: 242-250.

Gay RD, Clarke AW, Elgundi Z, Domagala T, Simpson RJ, Le NB, Doyle AG and Jennings PA (2010) Anti-TNFα domain antibody construct CEP-37247: Full antibody functionality at half the size. *MAbs* **2**: 625-638.

Gebauer M and Skerra A. (2009) Engineered protein scaffolds as next-generation antibody therapeutics. *Curr Opin Chem Biol* **13**: 245-55.

Hoeben BA, Molkenboer-Kuenen JD, Oyen WJ, Peeters WJ, Kaanders JH, Bussink J, and Boerman OC (2011) Radiolabeled cetuximab: dose optimization for epidermal growth factor receptor imaging in a head-and-neck squamous cell carcinoma model. *Int J Cancer* **129**: 870-878.

Hopp J, Hornig N, Zettlitz KA, Schwarz A, Fuss N, Müller D and Kontermann RE (2010) The effects of affinity and valency of an albumin-binding domain (ABD) on the half-life of a single-chain diabody-ABD fusion protein. *Protein Eng Des Sel* **23**: 827–834.

Hovgaard DJ, Folke M, Mortensen BT, Nissen NI (1994) Recombinant human interleukin-3: pharmacokinetics after intravenous and subcutaneous bolus injection and effects on granulocyte kinetics. *Br J Haematol* **87**:700-707.

Hovgaard D, Mortensen BT, Schifter S, Nissen NI (1992) Clinical pharmacokinetic studies of a human haemopoietic growth factor, GM-CSF. *Eur J Clin Invest* **22**:45-49.

Ishida T and Kiwada H (2008) Accelerated blood clearance (ABC) phenomenon upon repeated injection of PEGylated liposomes. *Int J Pharm* 354: 56-62.

Jevsevar S, Kunstelj M, and Porekar VG (2010) PEGylation of therapeutic proteins. *Biotechnol J* **5**: 113-28.

Lipovsek D (2011) Adnectins: engineered target-binding protein therapeutics. *Protein Eng Des Sel* **24**:3-9.

Nayak TK, Regino CA, Wong KJ, Milenic DE, Garmestani K, Baidoo KE, Szajek LP, and Brechbiel MW (2010) PET imaging of HER1-expressing xenografts in mice with 86Y-CHX-A"-DTPA-cetuximab. *Eur J Nucl Med Mol Imaging* **37**:1368-1376.

Nayak TK, Garmestani K, Baidoo KE, Milenic DE, Brechbiel MW (2010) Preparation, biological evaluation, and pharmacokinetics of the human anti-HER1 monoclonal antibody panitumumab labeled with ^{86}Y for quantitative PET of carcinoma. *J Nucl Med* **51**: 942-950.

Niu G, Li Z, Xie J, Le QT and Chen X (2009) PET of EGFR antibody distribution in head and neck squamous cell carcinoma models. *J Nucl Med* **50**:1116-1123.

Sato H (2002) Enzymatic procedure for site-specific pegylation of proteins. *Adv Drug Deliv Rev* **54**: 487-504.

Skerra A (2007) Alternative non-antibody scaffolds for molecular recognition. *Curr Opin Biotechnol* **18**: 295-304.

Stork R, Campigna E, Robert B, Müller D, and Kontermann RE (2009) Biodistribution of a bispecific single-chain diabody and its half-life extended derivatives. *J Biol Chem* **284**: 25612-25619.

Taguchi T (1986) Clinical studies of recombinant interferon alfa-2a (Roferon-A) in cancer patients. *Cancer* **57**: 1705-1708.

Tolcher AW, Sweeney CJ, Papadopoulos K, Patnaik A, Chiorean EG, Mita AC, Sankhala K, Furfine E, Gokemeijer J, Iacono L, Eaton C, Silver BA, and Mita M (2011) Phase I and pharmacokinetic study of CT-322 (BMS-844203), a targeted Adnectin inhibitor of VEGFR-2 based on a domain of human fibronectin. *Clin Cancer Res* **17**: 363-371.

Tolmachev V, Rosik D, Wållberg H, Sjöberg A, Sandström M, Hansson M, Wennborg A, and Orlova A (2010) Imaging of EGFR expression in murine xenografts using site-specifically labelled anti-EGFR ^{111}In-DOTA-Z EGFR: 2377 Affibody molecule: aspect of the injected tracer amount. *Eur J Nucl Med Mol Imaging* **37**: 613-622.

Veronese FM and Mero A (2008) The impact of PEGylation on biological therapies. *BioDrugs* **22**: 315-29.

DMD Fast Forward. Published on May 24, 2012 as DOI: 10.1124/dmd.112.044792
This article has not been copyedited and formatted. The final version may differ from this version.

FIGURE LEGENDS

Figure 1. **Schematic representation of a 40-kDa branched PEGylated Adnectin (P40B-EI-tandem).**

The tandem Adnectin targets both human EGFR and IGF-1R and the structure of the cross-linker (BMPS) between Adnectin and PEG is shown.

Figure 2. Synthesis and purification of the [^{14}C]-P40B-EI-tandem.

(A) Synthesis [^{14}C]-BMPS. The asterisk on the maleimide pyrrole ring indicates the position of the [^{14}C]-label. (B) Synthetic scheme of [^{14}C]-P40B-EI-tandem. (C) Purity of [^{14}C]-P40B-EI-tandem revealed by SDS-PAGE. Lane 1 and 4, molecular weight marker; lane 2, the purified EI-tandem eluted from Ni-NTA affinity column; lane 3, EI-tandem up-shifted to 100 kDa after conjugation with [^{14}C]-maleimide-P40B; lane 5, 6 and 7, 2, 6, 12 µg of purified [^{14}C]-P40B-EI-tandem. (D) Analysis of purity and specific radioactivity [^{14}C]-P40B-EI-tandem by size-exclusion gel filtration chromatography. Upper panel, UV trace of HPLC elution profile at A280 nm; lower panel, radioactivity trace of the same elution profile.

Figure 3. ***In vitro*** **cellular activity of [^{14}C]-P40B-EI-tandem.**

(A) Inhibition of EGFR phosphorylation in H292 cells. (B) Inhibition of IGF-IR phosphorylation in H292 cell.

Figure 4. Tissue distribution and tumor uptake of [^{14}C]-P40B-EI-tandem in H292 and RH41 tumor-bearing mice.

(A), (B), and (C) are representative whole-body autoradiograms of radioactivity distribution at respective 2, 24, and 53 h after IV dosing of [^{14}C]-P40B-EI-tandem (33 mg/kg; 1.7 μCi/mouse). (D) Uptake of radioactivity into RH41 and H292 tumors at 2, 24, and 53 h after IV dosing. (E) Tissue-to-blood radioactivity ratios at 2, 24 and 53 h after IV dosing to the tumor-bearing mice.

DMD Fast Forward. Published on May 24, 2012 as DOI: 10.1124/dmd.112.044792
This article has not been copyedited and formatted. The final version may differ from this version.

Table 1

Serum concentrations determined by radioactivity and ELISA methods after IV and IP administration of [^{14}C]-P40B-EI-adenctin (33 mg/kg)

Dose	[^{14}C]-P40B-EI-Adnectin						P40B-EI-Adnectin[c]	
	IV_33 mg/kg			IP_33 mg/kg			IP_10mg/kg	IP_100 mg/kg
Time	Rad.Act.[a]	ELISA[a]	Conc. Ratio Rad. /ELISA	Rad. Act.[a]	ELISA[a]	Conc. Ratio Rad. /ELISA	ELISA	
h	µM	µM		µM	µM (µM/mg/kg)		µM (µM/mg/kg)	
2	14, 16	7.8, 9.8	1.7	-	-	-		
8	-	-	-	14, 15	8.7, 9.3 (0.27)[b]	1.6	3.3 ± 0.1 (0.33)[b]	27 ± 2.6 (0.27)[b]
24	7.8, 7.2	4.5, 4.3	1.7	-	-	-		
48	4.7, 3.9	2.1, 1.7	2.3	5.0-5.2	2.0, 2.4 (0.066)[b]	2.3	0.4 ± 0.04 (0.04)[b]	7.7 ±1.1 (0.077)[b]
53	3.9, 4.0	1.6, 1.7	2.4	3.8, 4.3	1.5, 1.8 (0.05)[b]	2.3		

[a] Concentration from individual mouse.

[b] The data in the parenthesis are the dose-normalized average concentrations

[c] The exposures of the non-labeled P40B-EI-Adnectin were first reported by Emanuel et al. (2011).

Table 2

Tissue distribution of radioactivity in xenograft mice bearing H292 and RH41 tumors after a single IV dose of [^{14}C]-P40B-EI-tandem

Tissues	Radioactivity in tissue[a]		
	2 h	24 h	53 h
	(%ID/g tissue)		
Blood (heart)	27.9	14.3	6.2
Tumor (RH41)	1.1	1.9	2.6
Tumor (H292)	5.9	6.1	10.8
Brain	0.5	0.3	0.2
Bone marrow	5.2	3.5	2.1
Heart	9.3	4.3	2.2
Liver	6.8	5.9	10.6
Lung	16.1	8.4	3.6
Kidney (cortex)	6.2	6.8	7.5
Muscle	0.4	0.5	0.5

[a]The radioactivity in the tumors was calculated as the average radioactivity at the rim and in the center. The quantitation limit was 0.03% injected dose (ID) /g tissue.

Figure 1

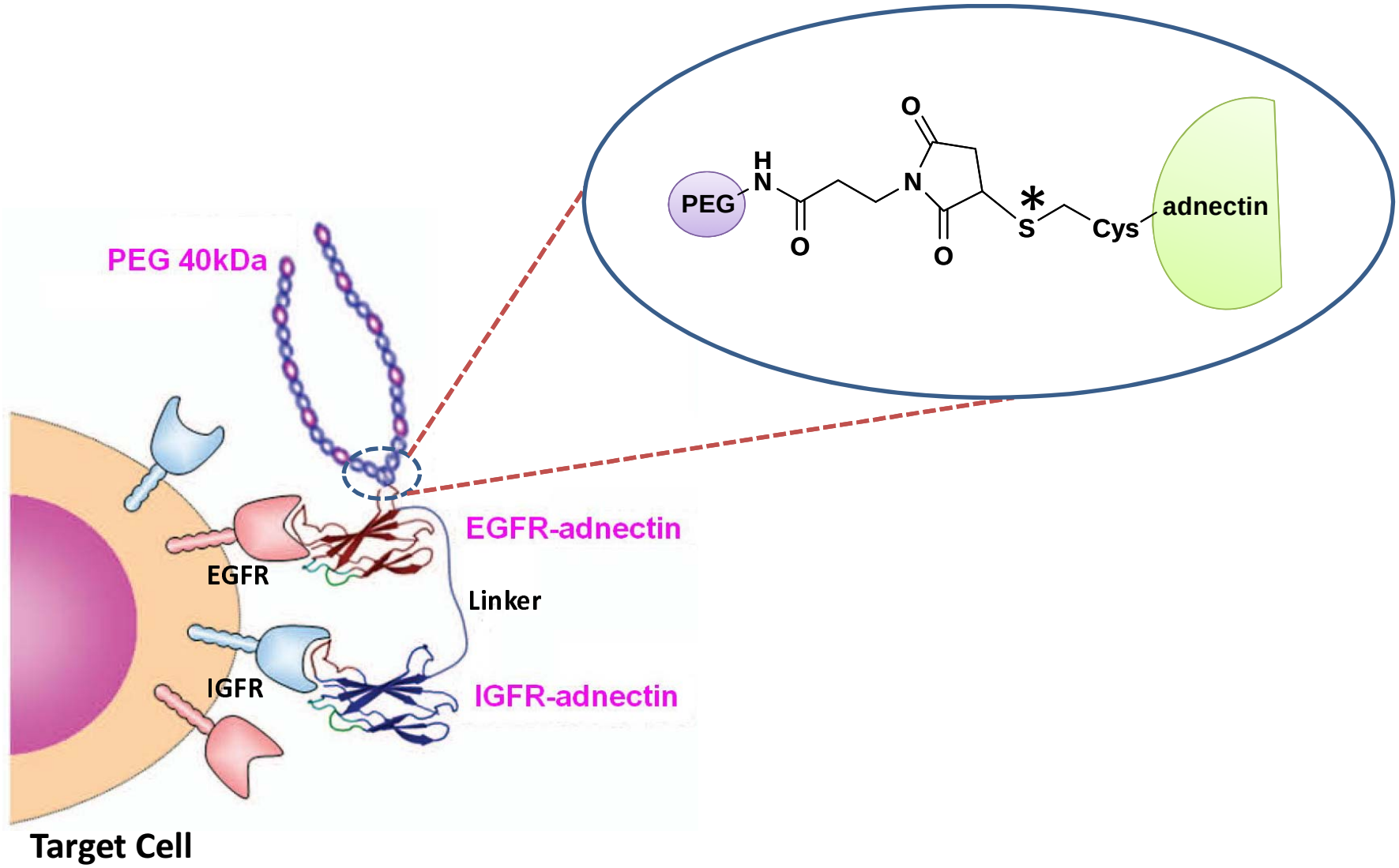

Figure 2

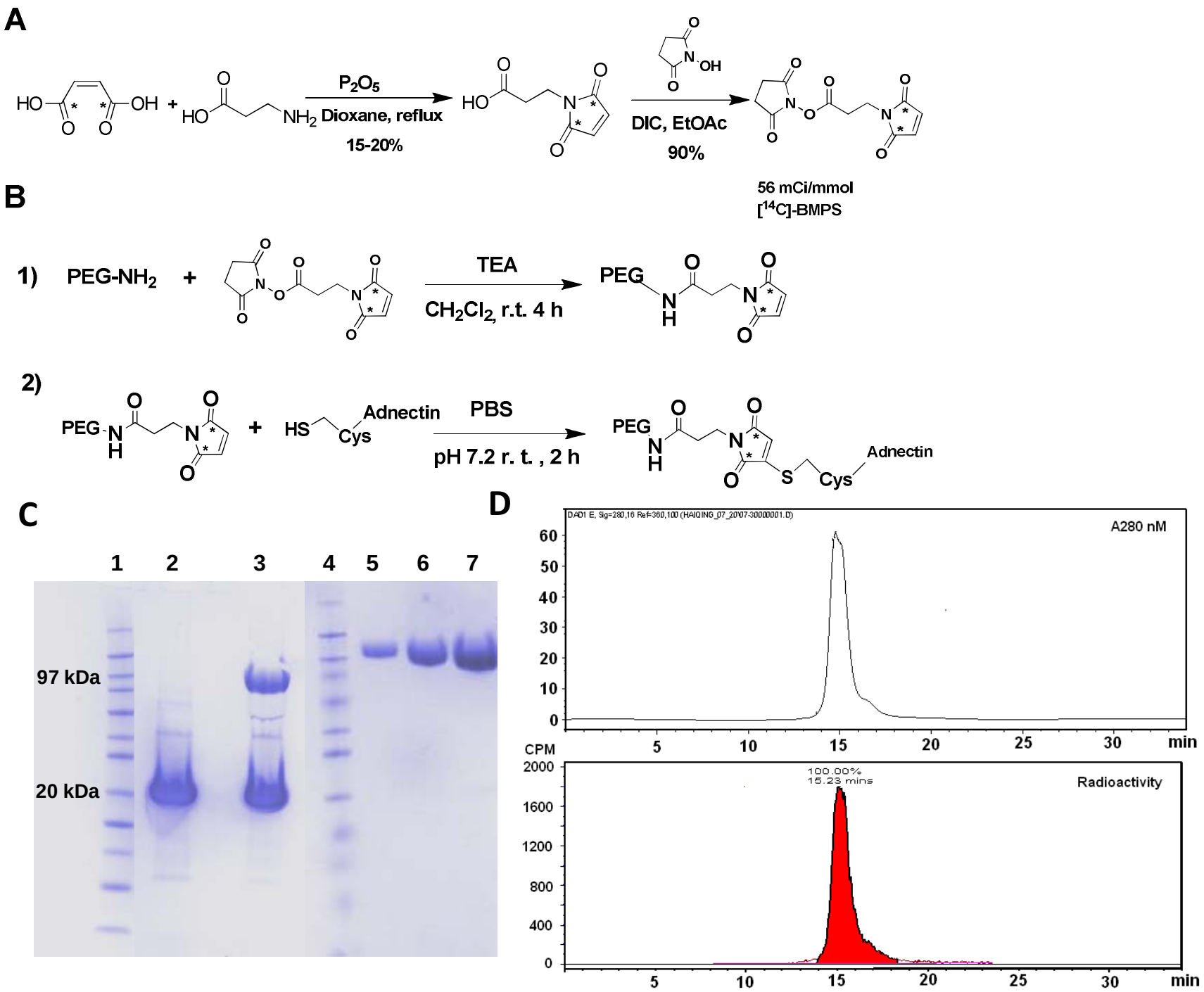

Figure 3

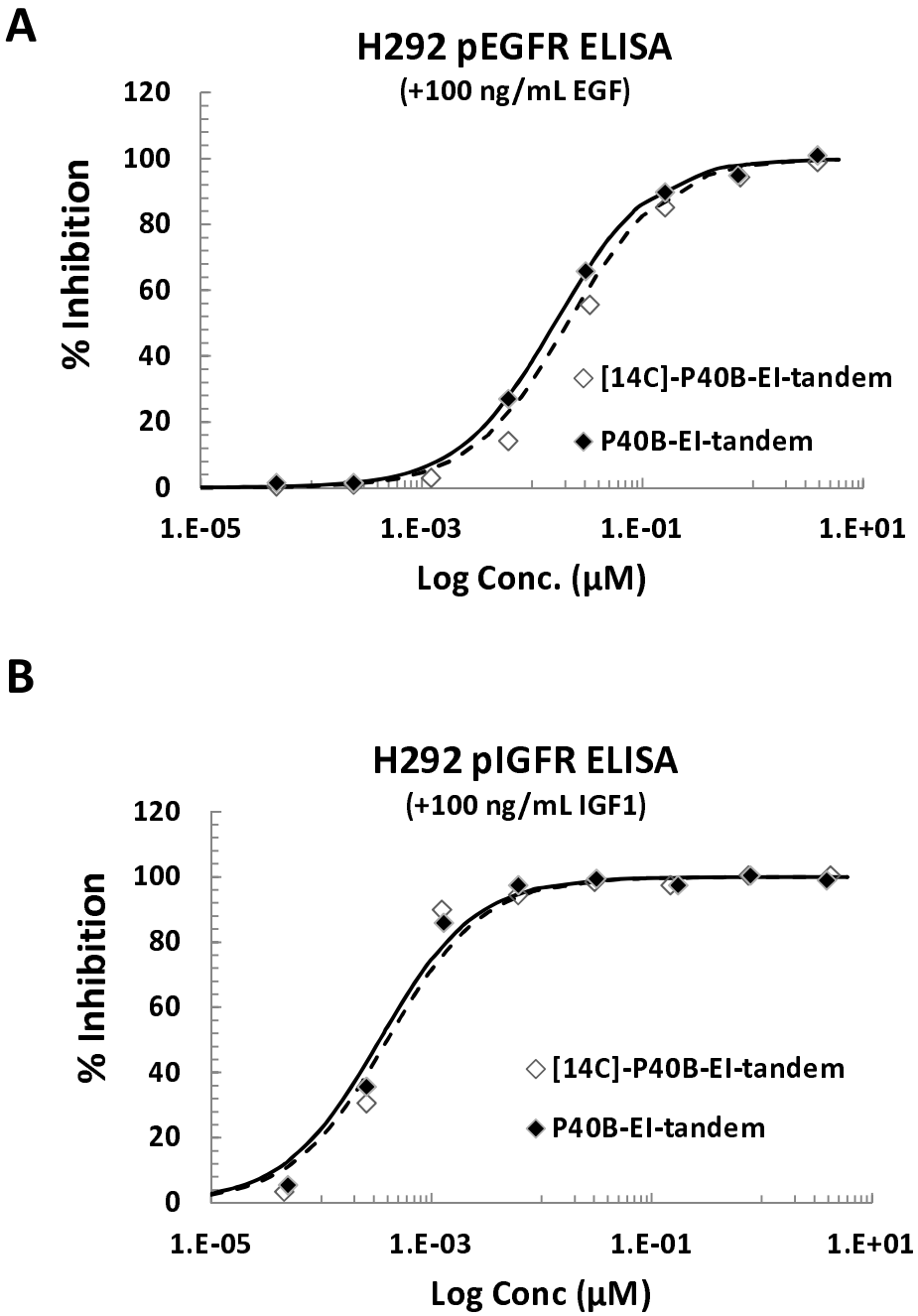

Figure 4